Electronic, Structural and Functional Versatility in Tetrathiafulvalene-Lanthanide Metal-Organic Frameworks

Javier Castells-Gil,[a] Samuel Mañas-Valero,[a] Iñigo J. Vitórica-Yrezábal,[b] Duarte Ananias,[c] João Rocha,[c] Raul Santiago,[d] Stefan T. Bromley,[d,e] José J. Baldoví,[f] Eugenio Coronado,[a] Manuel Souto*[a] and Guillermo Mínguez Espallargas*[a]

Abstract: Tetrathiafulvalene-Lanthanide (TTF-Ln) Metal-Organic Frameworks (MOFs) are an interesting class of multifunctional materials in which porosity can be combined with electronic properties such as electrical conductivity, redox activity, luminescence and magnetism. Herein we report a new family of isostructural TTF-Ln MOFs, denoted as **MUV-5(Ln)** (Ln = Gd, Tb, Dy, Ho, Er), exhibiting semiconducting properties as a consequence of the short intermolecular S⋯S contacts established along the chain direction between partially oxidised TTF moieties. In addition, this family shows photoluminescence properties and single-molecule magnetic behaviour, finding near-infrared (NIR) photoluminescence in the Yb/Er derivative and slow relaxation of the magnetisation in the Dy and Er derivatives. As such properties are dependent on the electronic structure of the lanthanide ion, we emphasise the immense structural, electronic and functional versatility of this class of materials.

Introduction

During the last decades, the emergence of Metal-Organic Frameworks (MOFs), porous crystalline materials constructed from metallic nodes and organic linkers, has attracted a large attention in view of their limitless structural and functional versatility giving rise to a wide range of potential applications.[1] Besides their intrinsic porosity, MOFs can incorporate electronic functionalities such electrical conductivity,[2,3] magnetism[4] and luminescence[5,6] from their inorganic and organic building blocks. This permits the fabrication of novel multifunctional materials that

[a] J. Castells-Gil, S. Mañas-Valero, Prof. E. Coronado, Dr. M. Souto, Dr. G. Mínguez Espallargas
     Instituto de Ciencia Molecular (ICMol), Universidad de Valencia
     c/ Catedrático José Beltrán 2, 46980 Paterna, Spain
     E-mail: manuel.souto@uv.es; guillermo.minguez@uv.es

[b] Dr. I. Vitórica-Yrezábal
     School of Chemistry, University of Manchester
     Oxford Road, Manchester M13 9PL, United Kingdom

[c] Dr. D. Ananias, Prof. J. Rocha
     Department of Chemistry and CICECO-Aveiro Institute of Materials
     University of Aveiro
     3810-193 Aveiro, Portugal

[d] Raul Santiago, Prof. S. T, Bromley
     Departament de Ciència de Materials i Química Física & Institut de Química Teòrica i Computacional, Universitat de Barcelona, Universitat de Barcelona, C/Martí i Franquès 1, E-08028 Barcelona, Spain

[e] Prof. S. T, Bromley
     Institució Catalana de Recerca i Estudis Avançats (ICREA), E-08010 Barcelona, Spain

[f] Dr. J. J. Baldoví
     Max Planck Institute for the Structure and Dynamics of Matter, Luruper Chaussee 149, D-22761 Hamburg, Germany

     Supporting information for this article is given via a link at the end of the document.

combine at the same time porosity with various physical properties.[7]

Tetrathiafulvalene(TTF)-based ligands are promising building-blocks for obtaining such materials since they can provide interesting features such as electrochemical properties or electrical conductivity.[8] TTF derivatives show a remarkable electron-donor character and they can form π-π stacks with relatively short S⋯S interactions to promote charge transport. For this reason, these systems have been widely studied as molecular conductors in the field of molecular electronics. In recent years, a variety of TTF-based MOFs have been reported to exhibit tunable electrical conductivity,[9,10] photo-induced spin-crossover,[11] enhanced catalytic activity[12] or breathing-dependent redox activity.[13,14]

On the other hand, lanthanide Metal-Organic Frameworks (Ln-MOFs) have also attracted a broad interest since they can exhibit interesting structural and chemical properties including magnetism and luminescence.[15] For example, trivalent lanthanide (Ln³⁺) MOFs exhibiting photoluminescence are promising materials with numerous applications for the development of sensors and light-emitting devices.[5,6] In addition, the incorporation of single-molecule magnetic (SMM) behaviour into a family of Ln-MOFs has been recently accomplished through the use of anisotropic magnetic ions[16,17] making these materials very interesting candidates for quantum computation and molecular spintronic applications[18].

In the last years, Pointillart *et al.* have described a variety of lanthanide coordination complexes bearing different TTF ligands which can exhibit multiple functionalities such as luminescence, redox properties and SMM behaviour.[19–21] In addition to their intrinsic redox properties, TTF-based ligands can act as both structural agent and organic chromophore isolating the magnetic centres and sensitising the lanthanide luminescence.[20] In this context, the three-dimensional organisation of these TTF-Ln complexes is encouraged in order to incorporate further functional properties such as electrical conductivity taking advantage of intermolecular interactions between partially oxidised TTF units.[9,22,23]

Along this line, two different TTF-Ln MOFs families exhibiting semiconducting and magnetic properties have been very recently reported.[23,24] However, the crystal structures of these materials show the formation of orthogonal TTF dimers or large intermolecular S⋯S distances, which are usually problematic for attaining a proper orbital overlap between the TTF moieties and, thus, limiting the charge delocalization. Herein, we present a family of isostructural TTF-Ln MOFs, achieved by an alternative synthetic procedure and named as **MUV-5(Ln)** (MUV: Materials of University of Valencia; Ln = Gd, Tb, Dy, Ho, Er), yielding a new crystal structure in which the TTF moieties are arranged in a parallel fashion and with relatively short S⋯S interactions enhancing the electronic coupling between TTF units, as

confirmed by transfer integral calculations. The TTF linkers are partially oxidised being responsible for charge transport and for the semiconducting behaviour of the MOF. In addition, photoluminescence properties and SMM behaviour have been studied for **MUV-5**. Such properties are dependent on the electronic nature of the lanthanide ion[26], evidencing a wide structural, electronic, and functional versatility for this new family of TTF-Ln MOFs.

Results and Discussion

Synthesis

MUV-5(Ln) was synthesised by means of an isoreticular approach through an adapted synthetic procedure described for the synthesis of MUV-4(Dy).[17] Solvothermal reaction of $Ln(OOCCH_3)_3$ and TTF-tetrabenzoic acid (H_4TTFTB) in a mixture of water and acetic acid at 170 ºC for 12 hours allowed the formation of single-crystals of **MUV-5** (Scheme 1). Two crystalline polymorphs were identified by Single-Crystal X-Ray Diffraction (SCXRD), namely **MUV-5a** and **MUV-5b**, of formulae $[Ln_3(TTFTB)_2(OOCCH_3)(OH)(H_2O)] \cdot 2.5H_2O$[27] and $[Ln(HTTFTB)(H_2O)] \cdot (CH_3COOH)$, respectively, whose formation depends on the amount of acetic acid used in the synthesis.
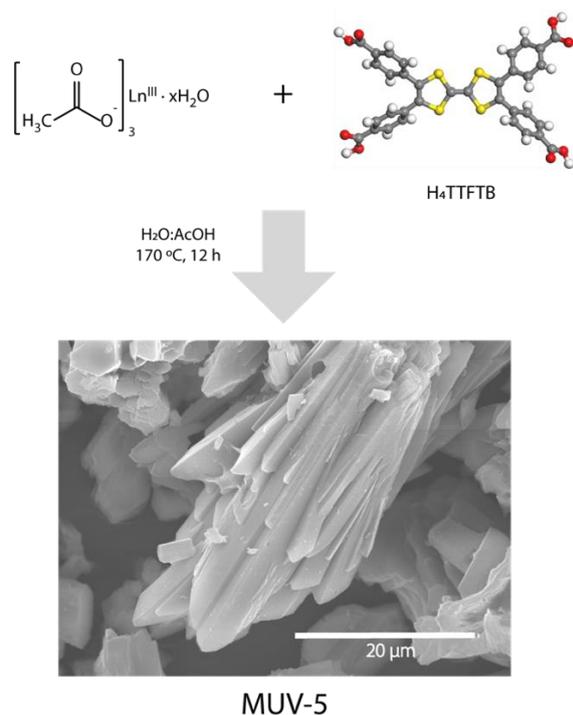
Scheme 1. Synthesis of **MUV-5a**

Crystal structure

MUV-5a crystallises in the monoclinic space group $P2/c$ (Tables S1 and S2). Two crystallographically independent Ln^{3+} ions are found in the asymmetric unit with different coordination environments. One of them is 7-coordinated with a capped trigonal prism geometry, whereas the second Ln^{3+} ion can be either 8 or 9-coordinated with a distorted triangular dodecahedron environment and spherical capped square antiprism, respectively, as calculated by the software SHAPE[25] (Figures S1 and S2). The difference between the 8 or 9-coordinated form in the latter relies on the position of the disordered acetate anion acting as a bridge between both Ln^{3+} ions (Figure 1b). The metallic secondary building unit (SBU) is composed of Ln^{3+} ions connected through bridging carboxylate bonds from the linker and acetate anions to form infinite Ln-carboxylate chain along the *a*-axis. The connection of these infinite Ln-carboxylate chains with the TTFTB linkers yields a 3D structure with two types of parallel 1D micropores extending along the *a*-axis that are filled with water molecules or coordinated acetate anions (Figure 1).
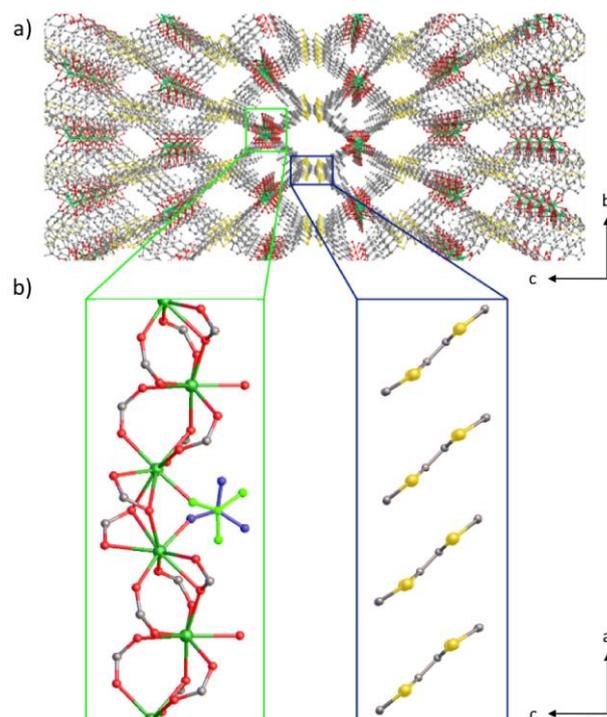

Figure 1. a) View of the crystal structure of **MUV-5a** along the *a*-axis and b) view of the arrangement of the Ln^{3+} ions (left) and TTF units (right) within the structure of **MUV-5a**. Colour code: C (grey), O (red), Ln (green), S (yellow). The disordered acetate anions have been highlighted as green and blue in order to show the two different orientations of the acetate molecules.

On the other hand, **MUV-5b** crystallizes in the monoclinic space group $P2_1/n$. Unlike **MUV-5a**, **MUV-5b** has a dimeric Ln_2 SBU similar to that observed in MUV-4a[17]. In this case, only one crystallographically independent Ln^{3+} ion is observed in the

asymmetric unit. Each Ln atom is 8-coordinated with a distorted triangular dodecahedron geometry (Figures S3 and S4). The structure of **MUV-5b** is built upon dimeric SBUs of formula $[Ln_2(H_2O)_2(\mu\text{-}O_2C)_2(O_2C)_4(HO_2C)_2]$ (Figure S5) in which the Ln^{3+} ions are kept at a distance of 4.88 Å connected by two bridging carboxylate groups. The coordination sphere of each Ln^{3+} ion is completed by other 5 oxygen atoms from 3 different carboxylate groups and one water molecule (Figure S5). Finally, structure of **MUV-5b** also displays two types of one-dimensional micropores filled with acetic acid (Figure S3).

Pure crystalline phase of **MUV-5a** was confirmed by Powder X-Ray diffraction (PXRD, Figures S7-S12) and Thermogravimetric Analysis (TGA) (Figure S13). LeBail refinement converged with very good residual values (R_{wp} = 5.58 %; R_p = 4.36 %, Figure S8, Table S3). The small one-dimensional micropores allow the structure to have a free volume of 24 % of the unit cell volume as calculated by Mercury[28] (Figure S14). In order to examine the porosity of these materials, gas sorption experiments were performed on **MUV-5a** which was previously activated at 150 °C under vacuum overnight. N_2 adsorption-desorption isotherms performed at 77 K reveals a minimum uptake of N_2, in line with other previously reported TTF-based coordination polymers.[29] Interestingly, **MUV-5a** is able to adsorb CO_2 with a modest CO_2 uptake of 65 $cm^3 \cdot g^{-1}$ (12.8 wt. %) at 273 K (Figure S15), which is higher than that observed in other similar TTF-based MOFs at 195 K[29], and a total uptake of 2.1 $mmol \cdot g^{-1}$ at 12 bar and 273 K (Figure 2). The selectivity of **MUV-5a** towards the adsorption of CO_2 over N_2 likely arises from the higher quadrupole moment of CO_2, which makes it capable of interacting more strongly with the framework.[29,30] This feature opens the way for the utilization of this type of materials in gas separation or sensing applications.
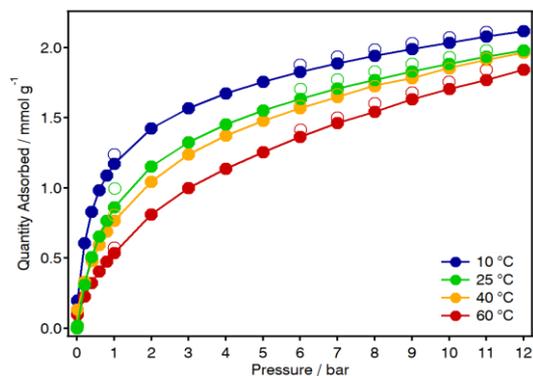
Figure 2. Adsorption (closed symbols) and desorption (open symbols) isotherms of CO_2 at different temperatures in **MUV-5a(Dy)**.

As far as the arrangement of the organic linkers is concerned, we note that in **MUV-5** solids the TTF units are forming one-dimensional segregated stacks of slightly slipped moieties running along the *a*-axis (Figures 1 and 3). However, there are important differences in both structures. First, the TTF struts in **MUV-5b** display a boat conformation with a central C=C distance of 1.32 Å and the dihedral angle between the planes formed by the two dithiol rings is 17° (Figure S6), suggesting that the TTF moiety is in the neutral state[31,32] (Figure 3a). On the other hand, the TTF moieties are packed along the *a*-axis with inter-centroid and S···S distances ranging from 4.40-4.90 Å and 3.92-4.27 Å, respectively. In contrast, in **MUV-5a** the TTF units adopt an S-shaped conformation with a central C=C bond distance of 1.34 Å, which is slightly longer than that in **MUV-5b** (Figure 3) and a dihedral angle of 5°, suggesting that the TTF units in **MUV-5a** are in the radical cation state (i.e. as TTF•+), or at least partially oxidised. It is important to note that neutral TTF has a boat-like conformation (C_{2v} symmetry) whereas TTF•+ moieties have a planar D_{2h} symmetry as a result of the 6 π-electron heteroaromaticity of the 1,2-dithiolium cation.[32,35] The partial oxidation of the TTF units in **MUV-5a** was confirmed by EPR measurements of the crystals at room temperature that show a signal with a g = 2.007, characteristic of organic radicals, and much more intense than the one for **MUV-5b** (Figure S16). As it has been observed in similar systems, TTF moieties in **MUV-5a** were at least partially oxidised during the MOF synthesis.[9] We hypothesise that this excess of positive charge is compensated through deprotonation of coordinated water molecules. Otherwise, the TTF units are stacked in a parallel manner nearly equally separated with inter-centroid distances ranging from 4.06 to 4.28 Å and being the closest S···S distances 3.61 and 3.86 Å (Figure 3b). These distances between the TTF units in **MUV-5a** are significantly shorter than in **MUV-5b**, and comparable to other TTF-based MOFs that display electrical conductivity.[9,10] This different arrangement with shorter intermolecular interactions between the partially oxidised TTF units in **MUV-5a** should be translated in a better orbital overlap between the linkers and, thus, in an enhancement in the conducting properties of the material that will be discussed below.
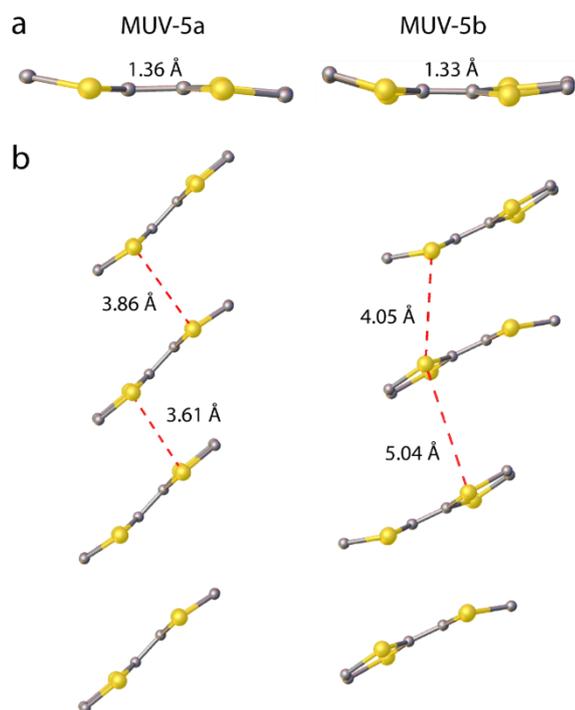
Figure 3. View of the a) conformation and b) arrangement of the TTF units within the structure of **MUV-5a** and **MUV-5b.** The red dashed lines show the shortest S···S distances between TTF pairs in **MUV-5(Dy)**.

Charge values for the TTF moieties in each structure were estimated by taking into account the bond length (C=C/C-S) ratio[34] obtaining values in the range from +0.1 to +0.7 suggesting that the TTF units are partially charged in **MUV-5a** (Table S5) in agreement with EPR spectroscopy. By contrast, the charge calculated in the case of **MUV-5b** indicate that TTF units are in the neutral state (q = 0). It should be noted that this correlation between charge and geometry is only approximate, although the estimated charges are in good agreement with the more planar conformation of the TTF units in **MUV-5a** (dihedral angle of 5˚), which is typical for TTF$^{+ \cdot}$ radical cation, whereas the boat-like conformation in **MUV-5b** (dihedral angle of 17˚) is similar to the one for neutral TTF.[32,35]

|	Conductivity (S·cm^{-1}) [a]	Shortest S···S distances (Å)
MUV-5a(Gd)	2.0x10^{-7}	3.73
MUV-5a(Tb)	1.5x10^{-5}	3.68
MUV-5a(Dy)	3.9x10^{-7}	3.61
MUV-5a(Ho)	6.7x10^{-6}	3.67
MUV-5a(Er)	7.4x10^{-6}	3.65
MUV-5b(Dy)	3.3x10^{-7}	4.05

[a] Conductivities measured using four-contact probe pressed pellets at room temperature of two independent samples. Errors in the Supporting Information.

Electrical conductivity

In view of the formation of parallel stacks and partial oxidation of the TTF linkers which could promote charge transport in **MUV-5a(Ln)**, transport measurements of the different samples were performed using four-contact probe pressed pellet devices from two independent batches (see Supporting Information for more information). The room temperature conductivities for **MUV-5a(Gd), MUV-5a(Tb)**, **MUV-5a(Dy)**, **MUV-5a(Ho)** and **MUV-5a(Er)** were found to be in the order of $10^{-5} – 10^{-7}$ S·cm^{-1} (see Table S4 and Figures S18-S29). Although ground boundaries in pressed pellets induce large resistance in comparison to single crystal measurements, the obtained values are comparable to the ones for other TTF-based MOFs also measured as pressed pellets[33] and around two orders of magnitude higher than those for a recently reported TTF-Ln MOF family which show similar electrochemical properties (Figure S30).[25] It is important to note that in our case electrical conductivity is achieved without the need of any doping process since TTF moieties are already partially oxidised during the synthesis, thus maintaining permanent porosity in the structures. On the other hand, electrical conductivity for **MUV-5b(Dy)** was measured to be in the order of 10^{-8} S·cm^{-1}, one order of magnitude lower than for **MUV-5a(Dy)** which is consistent with the presence of larger S···S intermolecular distances and the absence of oxidised TTF units.

Transfer integral calculations

In order to further understand the difference of conductivities in **MUV-5a** and **MUV-5b**, DFT based calculations of intermolecular transfer integrals for TTF units in **MUV-5** were performed. Transfer or hopping integrals (t) measure the overlap of the frontier orbitals (i.e. HOMOs or LUMOs) between adjacent molecules and thus provide an indication of the strength of intermolecular conduction pathways for electrons (for HOMOs) or holes (for LUMOs). These calculations were performed using the Gaussian09 package [36] employing the PBE0 [37] and B3LYP [38] hybrid functionals, with a 6-311+G(d,p) basis set. Transfer integrals between the TTF moieties in the MOFs were calculated in free space with no intervening metals at 0 K providing information about the overlap between the molecular orbitals of the TTF units through which charge transport is expected to occur. Calculations using both functionals provided consistent and comparable results (see Table S6) and we report B3LYP values hereafter. The transfer integrals for neutral **MUV-5a** were calculated to be t_1 = 90.6 and t_2 = 16.5 meV which are considerably higher than the ones for **MUV-5b** (t_1 = 60.5 and t_2 = 8.4 meV) (Figure 4) in agreement with the higher conductivity measured for **MUV-5a**. We have also compared these values with the ones calculated for the other two TTF-Ln systems reported by Dincă[24] and Zuo[25] in order to examine potential correlations between the calculated transfer integrals and measured electrical conductivities. Regarding the systems reported by Dincă,[24] the

transfer integral was calculated to be 86.1 meV between the TTF dimers. However, the transfer integrals are significantly lower (32.9 and 12.9 meV) between orthogonally displaced non-dimerised TTF units (see Figure S31) in this system. On the other hand, although in the family of materials reported by Zuo and co-workers[25] the TTF units are displaced in a parallel fashion, the transfer integrals are lower (61.5 and 48.6 meV) than those for **MUV-5a**. This difference could help to explain the lower electrical conductivity reported by Zuo *et al.* (10^{-8} – 10^{-9} S·cm^{-1}) as compared to that measured for **MUV-5a** (10^{-6} – 10^{-7} S·cm^{-1}).
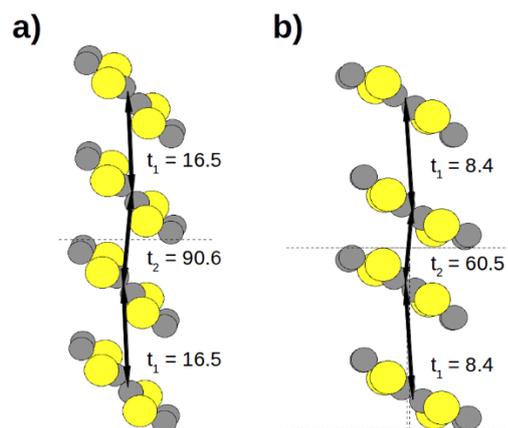
Figure 4. Schematic representation of TTF arrangements in the crystal structures of a) **MUV-5a** and b) **MUV-5b** indicating the transfer integrals (in meV).

Photoluminescence properties

To analyse the possible enhancement of photoluminescence via energy transfer among different lanthanide ions,[39] the mixed-lanthanide **MUV-5a(Yb$_{0.76}$Er$_{0.24}$)** was synthesized and characterized (see Supporting Information). The excitation spectra of **MUV-5a(Yb$_{0.76}$Er$_{0.24}$)**, **MUV-5a(Er)** and **MUV-5a(Gd)** compounds recorded at 295 K and 12 K (Figure 5) display a broad band from 250 to ca. 675 nm ascribed to the TTFTB^{4-} organic linker, covering most of the ultraviolet and visible spectral range. The spectra of **MUV-5a (Yb$_{0.76}$Er$_{0.24}$)** further display intense sharp lines in the 920-980 nm range assigned to the $^2F_{7/2} \rightarrow ^2F_{5/2}$ transition of Yb^{3+}. The poorer signal-to-noise ratio of **MUV-5a(Er)** sample spectra indicate that TTFTB ligand is more suited to sensitize Yb^{3+} than the Er^{3+} via the energy transfer process known as 'antenna effect'. Moreover, the Yb^{3+} emission may also be activated by direct excitation.
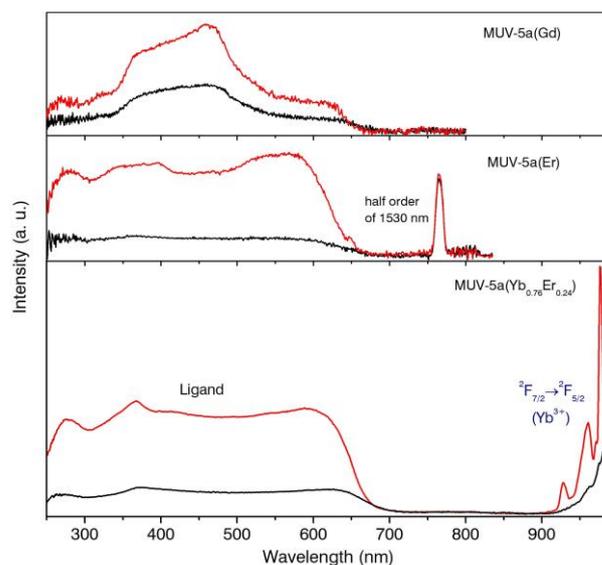
Figure 5. Excitation spectra of **MUV-5a (Yb$_{0.76}$Er$_{0.24}$)** ($\lambda_{Em.}$ = 1040 nm), **MUV-5a(Er)** ($\lambda_{Em.}$ = 1530 nm) and **MUV-5a(Gd)** ($\lambda_{Em.}$ = 1020 nm) recorded at 295 K (black lines) and at 12 K (red lines).

Upon ligand-mediated excitation at 560 nm, **MUV-5a(Yb$_{0.76}$Er$_{0.24}$)** (Figure 6) shows both intense emission in the 980-1050 nm region assigned to the Yb^{3+} $^2F_{5/2} \rightarrow ^2F_{7/2}$ transition, and faint emission peaking at 1530 nm assigned to the Er^{3+} $^4I_{13/2} \rightarrow ^4I_{15/2}$ transition. At 12 K, the well-defined sharp Stark components, resulting from the crystal-field splitting of the emitting states, demonstrate the crystallinity of the sample. Under the same excitation conditions, the emission of **MUV-5a(Er)** (Figure 6) is clearly weaker and dominated by a broad band ranging from *ca.* 940 to 1250 nm; the Er^{3+} $^4I_{13/2} \rightarrow ^4I_{15/2}$ transition is only prominent at 12 K. Because it is also present in the **MUV-5a(Gd)** spectra (Figure 6), the former band is attributed to the ligand's emission. The effective sensitization of the Yb^{3+} over the Er^{3+} emission is mainly due to a larger overlap between the ligand emission and the Yb^{3+} $^2F_{5/2}$ excited state, with an expected absorption cross-section at its maximum (976 nm) seven times larger than the resonant 980 nm Er^{3+} $^4I_{11/2}$ level.[40] The larger Yb^{3+} cross-section is often used to improve the Er^{3+} emission via Yb^{3+}-to-Er^{3+} energy transfer, including in Ln-bearing MOFs.[41,42] This is not observed for **MUV-5a(Yb$_{0.76}$Er$_{0.24}$)** presumably due to an effective quenching of the Er^{3+} emission prompted by the C-H, N-H and O-H high energy vibrations of the ligand and free water molecules. Such quenching effect is more relevant for the Er^{3+} emission because the energy gap between the corresponding emitting and fundamental level is significantly smaller, ca. 6510 cm^{-1} *vs.* 10200 cm^{-1} for Er^{3+} and Yb^{3+}, respectively. The 295 K and 12 K Yb^{3+} emission lifetime in **MUV-5a(Yb$_{0.76}$Er$_{0.24}$)** are 7±1 and 12±1 µs, respectively (Figure S33 in the Supporting Information).
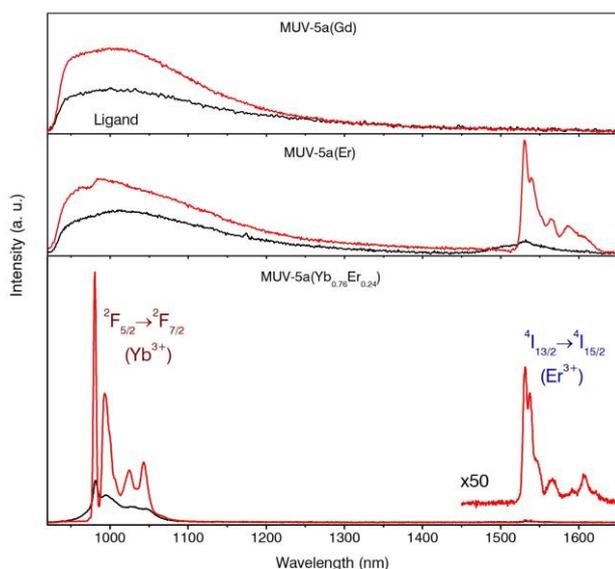
Figure 6. Emission spectra of **MUV-5a(Yb$_{0.76}$Er$_{0.24}$)** ($\lambda_{Exc.}$ = 560 nm), **MUV-5a(Er)** ($\lambda_{Exc.}$ = 560 nm) and **MUV-5a(Gd)** ($\lambda_{Exc.}$ = 430 nm) recorded at 295 K (black lines) and at 12 K (red lines).

Magnetic properties

Static magnetic measurements (dc) of **MUV-5a** solids were performed between 2 and 300 K under an applied field of 1000 G. The X_mT values at room temperature of **MUV-5a** are close to those expected for the free Ln ion, which indicates that most of the energy levels are populated at room temperature (Figure 7). The drop observed in X_mT at low temperatures is primarily ascribed to the depopulation of the highest energy levels, which is characteristic of anisotropic lanthanide ions. In case of **MUV-5a(Er)** there is a slight increase below 7 K, which may indicate the presence of weak dipolar ferromagnetic interactions.

The static magnetic susceptibility was simulated using the Radial Effective Charge[43] model, as implemented in the SIMPRE[44] computational package (See ESI for details), for all the **MUV-5a** solids. The full set of crystal field parameters, ground-J multiplet energy level schemes and main contributions to the wave functions are reported in Tables S8-12. According to our calculations, the predicted ground state for **MUV-5a(Dy1)** is mainly composed by $|\pm1/2\rangle$ (98.7%), whereas **MUV-5a(Dy2)** is characterized by 80% of $|\pm15/2\rangle$. This means that, in the case of Dy, the second crystallographic centre is the one responsible of the observed SMM behaviour. This situation is dissimilar to **MUV-5a(Er)**, where both crystallographic centres have a ground doublet characterized by high spin microstates (80.1% $|\pm13/2\rangle$ + 11.7% $|\pm15/2\rangle$ in the case of **Er1,** and 66.6% $|\pm15/2\rangle$ + 19.0% $|\pm9/2\rangle$ for **Er2**). However, the energy difference between the ground state and the first excited state in both centres is ~11 and 25 cm^{-1}, for **Er1** and **Er2**, respectively, which together with molecular and lattice vibrations may limit the performance of these systems as molecular nanomagnets.[45] On the other hand, the ground state of the different magnetic centres of **MUV-5a(Tb)**

and **MUV-5a(Ho)** are mainly characterized by $|0\rangle$ or a heavy mixture in the case of **Ho1**, which suggests the presence of fast relaxation processes.
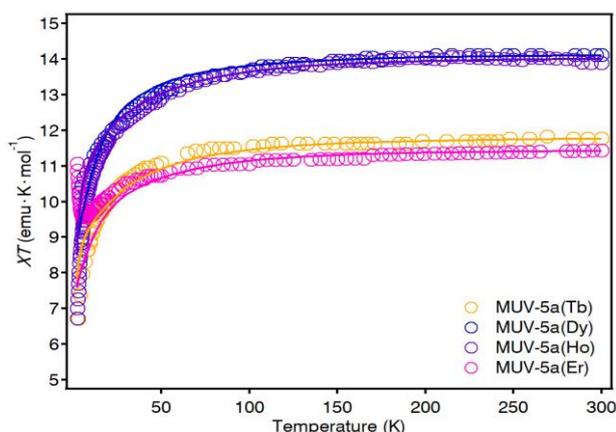
Figure 7. Experimental data (symbols) and theoretical simulation (lines) of the temperature dependence from 2 to 300 K of the magnetic susceptibility of **MUV-5a**. Tb (yellow), Dy (blue), Ho (purple) and Er (pink).

In order to demonstrate the differences in the magnetic behaviour of the different **MUV-5a** solids, we carried out dynamic (ac) magnetic measurements. As expected for **MUV-5a(Tb)** and **MUV-5a(Ho),** no out-of-phase signal (X'') can be observed at frequencies as high as 1000 Hz, even after applying an external dc magnetic field of 1000 G. In contrast, a frequency dependent out-of-phase signal is observed for **MUV-5a(Dy)** and **MUV-5a(Er)** as anticipated by the theoretical calculations (Figures S34 and S35). This is in agreement with the magnetic properties observed in similar Ln-MOFs.[25] However, no maximum in the out-of-phase signal can be observed above 2K, likely due to the presence of a very fast relaxation of the magnetization through a quantum tunnelling mechanism, as it has been previously suggested for other MOFs showing SMM behaviour.[17]

Conclusions

In summary, we have reported a new family of isostructural TTF-Ln MOFs, denoted as **MUV-5(Ln)**, which shows enhanced electrical semiconducting properties due to an effective 1D packing of the TTF moieties as confirmed by transfer integral calculations. In addition, near-infrared photoluminescence and slow relaxation of the magnetisation were investigated in different **MUV-5** solids which can be finely tuned by suitable choice of the Ln ions, thus giving rise to a new family of versatile functional MOFs showing different properties within the same material at the same time. Current research is focused on the synergism between different physical properties, such as conductivity and luminescence, as well as on the influence of the trapped molecules on these physical properties. We are confident that our findings will help to broaden the family of MOF featuring tailored functionalities.

Experimental Section

General methods and materials, crystal data, chemical characterisation, electrical measurements, transfer integral calculations, photoluminescence, magnetic measurements and calculations are available in the Supporting Information.

Acknowledgements

[1]   G. Maurin, C. Serre, A. Cooper, G. Férey, *Chem. Soc. Rev.* **2017**, *46*, 3104–3107.
[2]   L. Sun, M. G. Campbell, M. Dincă, *Angew. Chem. Int. Ed.* **2016**, *55*, 3566–3579.
[3]   I. Stassen, N. Burtch, A. Talin, P. Falcaro, M. Allendorf, R. Ameloot, *Chem. Soc. Rev.* **2017**, *46*, 3185–3241.
[4]   G. Mínguez Espallargas, E. Coronado, *Chem. Soc. Rev.* **2018**, 533–557.
[5]   J. Rocha, L. D. Carlos, F. A. A. Paz, D. Ananias, *Chem. Soc. Rev.* **2011**, *40*, 926–940.
[6]   W. P. Lustig, S. Mukherjee, N. D. Rudd, A. V. Desai, J. Li, S. K. Ghosh, *Chem. Soc. Rev.* **2017**, *46*, 3242–3285.
[7]   B. Li, H. M. Wen, Y. Cui, W. Zhou, G. Qian, B. Chen, *Adv. Mater.* **2016**, *28*, 8819–8860.
[8]   H.-Y. Wang, L. Cui, J.-Z. Xie, C. F. Leong, D. M. D'Alessandro, J.-L. Zuo, *Coord. Chem. Rev.* **2017**, *345*, 342–361.
[9]   T. C. Narayan, T. Miyakai, S. Seki, M. Dincă, *J. Am. Chem. Soc.* **2012**, *134*, 12932–12935.
[10]   S. S. Park, E. R. Hontz, L. Sun, C. H. Hendon, A. Walsh, T. Van Voorhis, M. Dincă, *J. Am. Chem. Soc.* **2015**, *137*, 1774–1777.
[11]   H.-Y. Wang, J.-Y. Ge, C. Hua, C.-Q. Jiao, Y. Wu, C. F. Leong, D. M. D'Alessandro, T. Liu, J.-L. Zuo, *Angew. Chem. Int. Ed.* **2017**, *56*, 5465–5470.
[12]   M. Souto, A. Santiago-Portillo, M. Palomino, I. J. Vitórica-Yrezábal, B. J. C. Vieira, J. C. Waerenborgh, S. Valencia, S. Navalón, F. Rey, H. García, G. Mínguez Espallargas, *Chem. Sci.* **2018**, *9*, 2413–2418.
[13]   J. Su, S. Yuan, H.-Y. Wang, L. Huang, J.-Y. Ge, E. Joseph, J. Qin, T. Cagin, J.-L. Zuo, H.-C. Zhou, *Nat. Commun.* **2017**, *8*, 2008.
[14]   M. Souto, J. Romero, J. Calbo, I. J. Vitorica-Yrezabal, J. L. Zafra, J. Casado Cordón, E. Ortí, A. Walsh, G. Mínguez Espallargas, *J. Am. Chem. Soc.* **2018**, *140*, 10562–10569.
[15]   D. M. P. Mingos, *Lanthanide Metal-Organic Frameworks*, Springer-Verlag Berlin Heidelberg, **2015**.
[16]   J. J. Baldoví, E. Coronado, A. Gaita-Ariño, C. Gamer, M. Giménez-Marqués, G. Mínguez Espallargas, *Chem. Eur. J.* **2014**, *20*, 10695–10702.
[17]   J. Castells-Gil, J. J. Baldoví, C. Martí-Gastaldo, G. Mínguez Espallargas, *Dalt. Trans.* **2018**, *47*, 14734–14740.
[18]   A. Gaita-Ariño, F. Luis, S. Hill, E. Coronado, *Nat. Chem.* **2019**, *11*, 301–309.
[19]   F. Pointillart, B. Le Guennic, S. Golhen, O. Cador, L. Ouahab, *Chem. Commun.* **2013**, *49*, 11632–11634.
[20]   F. Pointillart, B. Le Guennic, O. Cador, O. Maury, L. Ouahab, *Acc. Chem. Res.* **2015**, *48*, 2834–2842.
[21]   F. Pointillart, J. Jung, R. Berraud-pache, B. Le Guennic, V. Dorcet, O. Cador, O. Maury, Y. Guyot, S. Decurtins, S. Liu, et al., *Inorg. Chem.* **2015**, *54*, 5384–5397.
[22]   M. Bendikov, F. Wudl, D. F. Perepichka, *Chem. Rev.* **2004**, *104*, 4891–4945.
[23]   C. Rovira, *Chem. Rev.* **2004**, *104*, 5289–5317.
[24]   L. S. Xie, M. Dincă, *Isr. J. Chem.* **2018**, *2139*, 1119–1122.
[25]   J. Su, T. Hu, R. Murase, H. Wang, D. M. D'Alessandro, M. Kurmoo, J. Zuo, *Inorg. Chem.* **2019**, *58*, 3698–3706.
[26]   J. J. Baldoví, S. Cardona-Serra, J. M. Clemente-Juan, E. Coronado, A. Gaita-Ariño, A. Palii, *Inorg. Chem.* **2012**, *51*, 12565–12574.
[27]   Formula of **MUV-5a(Dy)** is [$Dy_3(TTFTB)_2(OOCCH_3)(OCHN(CH_3)_2$] having a coordinated DMF instead of H_2O/OH since these crystals were not properly washed and activated by heating.
[28]   C. F. Macrae, P. R. Edgington, P. McCabe, E. Pidcock, G. P. Shields, R. Taylor, M. Towler, J. van de Streek, *J. Appl. Cryst.* **2006**, *39*, 453–457.
[29]   B. Chen, Z. P. Lv, C. F. Leong, Y. Zhao, D. M. D'alessandro, J. L. Zuo, *Cryst. Growth Des.* **2015**, *15*, 1861–1870.
[30]   B. Liu, B. Smit, *Langmuir* **2009**, *25*, 5918–5926.
[31]   T. J. Kistenmacher, T. E. Phillips, D. O. Cowan, *Acta Cryst.* **1974**, *B30*, 763–768.
[32]   V. Mukherjee, N. P. Singh, *Spectrochim Acta A Mol Biomol Spectrosc* **2014**, *117*, 315–322.
[33]   L. Sun, S. S. Park, D. Sheberla, M. Dincă, *J. Am. Chem. Soc.* **2016**, *138*, 14772–14782.
[34]   T. C. Umland, S. Allie, T. Kuhlmann, P. Coppens, *J. Phys. Chem.* **1988**, *92*, 6456–6460.
[35]   S. Vela, M. Souto, I. Ratera, C. Rovira, J. Veciana, *J. Phys. Chem. A* **2016**, *120*, 10297–10303.
[36]   M. J. Frisch, *Gaussian 09, Revision B.01, Gaussian, Inc., Wallingford CT*, **2016**.
[37]   A. D. Becke, *J. Chem. Phys.* **1993**, *98*, 5648–5652.
[38]   C. Adamo, V. Barone, *J. Chem. Phys.* **1999**, *110*, 6158–6170.
[39]   S. Abednatanzi, P. Gohari Derakhshandeh, H. Depauw, F.-X. Coudert, H. Vrielinck, P. Van Der Voort, K. Leus, *Chem. Soc. Rev.* **2019**, *48*, 2535–2565.
[40]   C. Strohhöofer, A. Polman, *Opt. Mater.* **2013**, *21*, 705–712.
[41]   K. A. White, D. A. Chengelis, K. A. Gogick, J. Stehman, N. L. Rosi, S. Petoud, *J. Am. Chem. Soc.* **2009**, *131*, 18069–18071.
[42]   F. Artizzu, F. Quochi, L. Marchiò, E. Sessini, M. Saba, A. Serpe, A. Mura, M. L. Mercuri, E. Bongiovanni, P. Deplano, *J. Phys. Chem. Lett.* **2013**, *4*, 3062–3066.
[43]   J. J. Baldoví, J. J. Borrás-Almenar, J. M. Clemente-Juan, E. Coronado, A. Gaita-Ariño, *Dalt. Trans.* **2012**, *41*, 13705–13710.
[44]   J. J. Baldoví, S. Cardona-Serra, J. M. Clemente-Juan, E. Coronado, A. Gaita-Ariño, A. Palii, *J. Comput. Chem.* **2013**, *34*, 1961–1967.
[45]   L. Escalera-Moreno, J. J. Baldoví, A. Gaita-Ariño, E. Coronado, *Chem. Sci.* **2018**, *9*, 3265–3275.